Journal of Structural Geology 32 (2010) 1732–1741

Contents lists available at ScienceDirect

Journal of Structural Geology

journal homepage: www.elsevier.com/locate/jsg

Unlocking the effects of friction on fault damage zones

Heather M. Savage [a,*], Michele L. Cooke [b]

[a] Earth and Planetary Science Department, University of California, Santa Cruz, CA 95064, USA
[b] Geosciences Department, University of Massachusetts, Amherst, MA, USA

ARTICLE INFO

Article history:
Received 30 January 2009
Received in revised form
10 August 2009
Accepted 25 August 2009
Available online 11 September 2009

Keywords:
Fault zone evolution
Slip-weakening friction
Off-fault damage
Boundary element modeling

ABSTRACT

Two-dimensional, numerical models of a linear fault embedded within a linear elastic medium show the generation of off-fault tensile failure that results from inelastic slip along the fault. We explore quasi-static models with slip-weakening friction to assess the effects of spatially and temporally variable friction on the damage patterns. Tensile fractures form where tangential normal stresses along the fault exceed the tensile strength of the rock. These stresses result from locally high slip gradients at the rupture tip. Because faults of different displacement history and rock type could have varying slip-weakening distances, we examine the effect of changing the slip-weakening distance on the damage pattern and find that this parameter is important in determining off-fault fracture intensity and continuity along strike. Faults with short slip-weakening distance produce greater off-fault damage and significantly greater seismic radiated energy than faults with longer slip-weakening distances. We also investigate the effect of pre-existing damage on the subsequent development of fractures in second generation slip episodes and find that damage localizes onto pre-existing patches. These results could guide field studies of small faults as to whether the fault failed in one slip event or multiple small events.

1. Introduction

Halos of pervasive cracking around faults, called damage zones, are ubiquitous features (e.g. Brock and Engelder, 1977; Chester and Logan, 1986; Faulkner et al., 2006). Although damage zones have important implications for rupture dynamics (Rice et al., 2005) and fluid flow in fault zones (Caine et al., 1996), our understanding of their initiation and development is limited. The processes at work during fault slip that could contribute to damage of the host rock include: change in the quasi-static stress field, ground shaking due to seismic waves, fault geometry (such as fault bends), and frictional variability along the fault due to the frictional evolution of fault surfaces and/or gouge layers. However, damage zones nucleate and evolve from repeated deformation and displacement along faults (Sibson, 1977; Chester and Logan, 1986; Cowie and Shipton, 1998; Shipton and Cowie, 2003; Kim et al., 2004; Okubo and Schultz, 2005) and the overprinting of multiple events obscures how damage is generated in a single event, when the host rock is relatively intact. In order to understand how the damage zone develops in early stages of fault displacement when damage patterns should be more straightforward, we perform numerical experiments of the incipient stages of off-fault fracture development, on several-meter long faults that slip fractions of centimeters.

This study highlights some potential differences in macroscopic damage patterns and intensity between faults with varying initial roughness. Surface roughness will determine the critical slip distance, which is the slip distance required for a fault to renew asperity contacts so that friction can evolve between steady-state values. In this paper we are specifically modeling this process solely as a function of slip and will refer to this distance as the slip-weakening distance (L). This distance is most likely a function of fault maturity on natural faults. Incipient faults have rougher surfaces that smooth with shear displacement (Sagy et al., 2007). For faults with gouge layers, localization of slip into shear bands will have smaller critical slip distances compared to gouge zones in which the entire layer participates in shear (Marone and Kilgore, 1993). The length of the critical slip distance affects the variability of friction along the fault during failure. As the fault begins to slip, patches of the fault that have slipped more than the critical slip distance will be weaker than patches that have not and therefore faults with small critical slip distances will have greater difference in friction between adjacent segments. This frictional variability will in turn influence the slip gradient along the fault (e.g. Burgmann et al., 1994). When slip gradients are high enough, local tensile stresses can arise and off-fault fracturing commences (Cooke, 1997). Although critical slip distances may scale non-linearly with displacement along faults at large slips (Ohnaka, 2000;

* Corresponding author. Tel.: +1 831 459 5263.
E-mail address: hsavage@pmc.ucsc.edu (H.M. Savage).

0191-8141/$ – see front matter © 2009 Elsevier Ltd. All rights reserved.
doi:10.1016/j.jsg.2009.08.014

Abercrombie and Rice, 2005), they should be constant in terms of displacement for the small slip events we discuss in this paper.

Previous models of damage zone generation show that tensile tail cracks form in the tensile quadrants of the fault during displacements (e.g. Rispoli, 1981; Martel, 1997). Quasi-static models predict that fractures generally form at crack tips, which we refer to as fault tips in this paper in order to distinguish from the crack tips associated with off-fault damage. If present, an inelastic process zone can allow cracks to form inboard of the fault tip due to the slip gradient created at this change in frictional strength (e.g. Burgmann et al., 1994; Cooke, 1997). Dynamic slip studies have shown that the slip gradient preceding a rupture front produces fractures far inboard of the fault tip (Yamashita, 2000; Dalguer et al., 2003; Andrews, 2005). In these models, the zone of damage generated is thinnest where the rupture begins and widest at the end of the rupture in the tensile quadrants. The angle of the tail crack with respect to the main shear fracture can be a function of the strength of the process zone (Cooke, 1997) or in the case of dynamic rupture, slip velocity (Broberg, 1999). Yamashita (2000) predicted that joints formed in the tensile quadrant make a more oblique angle to the fault than joints formed in the compressive quadrant, however their fractures must fall along a prescribed regular mesh. These models predict that the generation of off-fault damage slows rupture propagation during an earthquake, as energy is absorbed through the creation of new fractures (e.g. Andrews, 2005).

In this paper, we directly simulate off-fault damage in the form of tensile fractures generated along small faults. Our model is quasi-static and has fault elements with a slip-weakening failure criterion. By studying a quasi-static slip-weakening frictional fault, we can isolate the effects of friction from the effects of dynamic stresses included in elastodynamic rupture models (e.g. Dalguer et al., 2003; Rice et al., 2005). We investigate fracture patterns for different slip-weakening lengths in an effort to distinguish how the early frictional properties of the fault influence the development of a damage zone. Although slip-weakening distance is a proxy for fault surface roughness, it does not reflect changes in fault planarity. Because our model is not constrained by a pre-existing mesh along which fractures have to form, these numerically generated fracture patterns can be compared with field-based measurements of macroscopic fractures.

Pre-existing damage may affect the slip distribution as well. The formation of fractures alter the properties of the fault zone that effect rupture propagation and subsequent failures, such as: reducing stiffness of the host rock, absorbing energy through the creation of new surfaces, and, once the rock becomes highly fractured, providing additional material to crush into gouge. Rupture branching may result from activation of shear fractures off the main fault (Rice et al., 2005). Manighetti et al. (2004) suggested that slip profiles along a fault are modulated by pre-existing damage. We investigate the second episode of slip by inserting the damage patterns from the initial models in our study and re-slipping the fault.

In addition to the fracture analysis, we investigate the effect of damage zone generation, as well as frictional variability on the fault system and the propagating rupture, by assessing the mechanical work budget. Work budget analyses examine the balance between the external work done on the system (stemming from stress and displacement at the boundaries) and the work consumed within the system by different deformational processes (e.g. Mitra and Boyer, 1986; Kanamori and Heaton, 2000; Cooke and Murphy, 2004; Abercrombie and Rice, 2005; Chester et al., 2005; Del Castello and Cooke, 2007; Ismat, 2008). Examining how elements of the work budget change as off-fault fractures grow provides insights into the tradeoffs among the deformational processes. Additionally, we can assess how development of damage zones changes the mechanical efficiency of faults on a systemic level.

2. Methods

2.1. Numerical method

Numerical models based upon continuum mechanics have been used to model various geologic processes such as earthquake triggering (e.g. Stein, 1999) and fault interaction (e.g. Willemse et al., 1996; Maerten et al., 1999; Savage and Cooke, 2004; Marshall et al., 2008). Mechanical models are based upon the three governing equations of continuum mechanics, i.e. the equilibrium, compatibility and constitutive equations (Crouch and Starfield, 1990).

The Boundary Element Method (BEM) is a numerical formulation of the governing equations. BEM models consider discontinuities (e.g. faults) in an otherwise elastic homogenous space. In two dimensions, fault surfaces and boundaries are discretized into linear elements. Tractions or displacements are prescribed for each element. Analytical functions calculate the effect of an element's traction or displacement on the rest of the elements within the model. These analytical functions form a system of linear equations that determines the resultant displacement or traction when the prescribed displacement or traction is summed with the influence of the other elements. Once the internal and external boundary tractions or displacements are known, the tractions or displacement for any point within the body can be calculated. This method is less computationally expensive than other methods such as Finite Element Method codes, which discretize the entire elastic body.

Fric2D is a two-dimensional, open-source BEM code that simulates deformation around fractures using the displacement discontinuity method (Crouch and Starfield, 1990) and incorporates a frictional failure criterion for fault slip, as well as fracture propagation (Cooke, 1997). In the Fric2D code, inelastic slip begins when the shear stress along the fault equals or exceeds the frictional strength of the element as defined by the Coulomb criterion:

$$\tau_c \leq c + \sigma_n \mu_s \tag{1}$$

where c is cohesion, μ_s is static friction, σ_N is normal traction (compression is positive) and τ_c is shear strength. Here, we have modified the failure criterion so that once the static frictional strength has been exceeded and the element commences inelastic slip, the frictional strength of the element decreases linearly as a function of slip, s:

$$\mu = \mu_s - \frac{s(\mu_s - \mu_d)}{L} \tag{2}$$

where μ_d is a prescribed dynamic friction value and L is the slip-weakening distance. Once the element has slipped the length of L, the frictional strength of the element will remain at the dynamic friction value. Slip-weakening friction is a simplistic friction law in the sense that it does not capture velocity dependence or memory effects on friction (Dieterich, 1979; Ruina, 1983). However, slip-weakening friction is adequate for dynamic rupture simulations where earthquake cycles are not relevant and has been used previously to study off-fault fracturing (Dalguer et al., 2003).

2.2. Model setup

We chose our boundary conditions to reflect the conditions on a fault at seismogenic depths subjected to shear stresses that are close to the frictional strength of the center patch of the fault (reflecting that this part of the fault is critically stressed). Our boundary conditions simulate simple shear conditions with constant shear and normal displacements along the top of the body and linearly decreasing displacements along the sides of the body,

with zero displacement along the bottom edge (Fig. 1). Normal displacements are calculated to reflect the lithostatic stress associated with a fault buried approximately 5 km (125 MPa). Displacement is applied in one step and changes in stress and displacement in the ensuing iterations represent the system reaching convergence. At each iteration, the friction coefficient evolves along the fault (Eq. (2)), elements along the fault slip (Eq. (1)) and new elements are added to simulate damage production. The fault is 15.1 m long and horizontal. The fault and the boundaries are discretized into equal-length 5 cm long linear elements. This element length provides satisfactory resolution of rupture advancement while limiting computational load. Along the fault, we prescribe a 3.1 m long center patch that is slightly frictionally weaker, so that the center patch fails first. In this way, we create a nucleation patch along which the rupture begins and propagates toward either end of the fault. The center patch is long enough to induce unstable sliding along the entire fault. The shear displacements along the boundaries of the model are chosen so that the center weak patch ($\mu = 0.28$) is at failure. The subsequent reduction of friction coefficient from 0.28 to 0.2 along the center patch during slip provides a shear stress drop of 10 MPa. The sides of the fault have higher prescribed friction coefficient, 0.32, and slip in response to the stress drop on the center patch.

Because rocks are weakest in tension, we choose to investigate areas likely to produce opening-mode cracks. New tensile fractures grow where the tangential normal stresses along a fault element exceed the tensile strength of the host rock, prescribed here as 15 MPa. Tensile stresses along the fault occur due to slip gradients between elements. Because our model does not have a pre-existing mesh, fractures are free to form at any orientation and nucleate perpendicular to the local maximum tensile direction. Fractures can form at the nodes between every other element and can grow by one element length during each iteration of frictional slip. The minimum spacing of off-fault fractures is 10 cm in these models. Propagation continues until the stress intensity factor (K_I) at the tip of the fractures is less than the fracture toughness (K_{Ic}), prescribed here as 2.5 MPa $m^{1/2}$. New fractures are permitted to open and slide with frictional resistance equal to the static friction value of the fault element that spawned the new fracture. Fractures are not allowed to interpenetrate.

2.3. Analysis of mechanical work

Total work of the fault system describes all of the energy expended during tectonic deformation of the fault and the surrounding host rock. Energy is consumed during deformation from work against gravity (W_{grav}), propagation of new surfaces (W_{prop}), work to overcome frictional resistance to sliding along the fault (W_{fric}), work that promotes ground motion in the form of seismic radiation (W_{seis}), and finally work that goes into off-fault deformation which we refer to as an internal strain energy (W_{int}). The total work reflects the summation of each of these components:

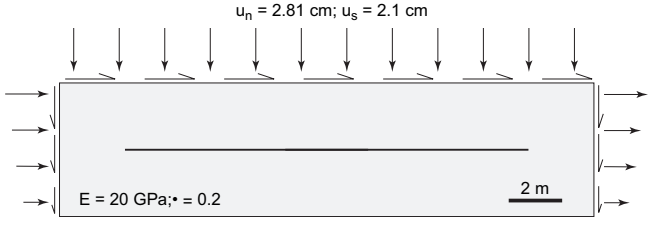

Fig. 1. Schematic diagram of model setup. Black horizontal line is the 3.1 m long critically stressed portion of the fault, which is otherwise shown as grey line.

$$W_{tot} = W_{grav} + W_{prop} + W_{fric} + W_{seis} + W_{int} \quad (3)$$

Each component of the total work done on the fault system can be evaluated from our model. In our analyses, we do not consider the effects of gravity because our fault is horizontal and our surface has no topography. The deformational work budget can be delineated in a variety of ways. Here we follow that used by Mitra and Boyer (1986), Cooke and Murphy (2004), Del Castello and Cooke (2007) and Ismat (2008). The result is very similar to the energy budget delineated by Kanamori and Heaton (2000) and Abercrombie and Rice (2005). Both approaches consider the same energy budget but divide the energy terms up in slightly different ways based on a difference in observables. As we describe each term we point out the differences in the notations.

The external work represents the amount of work applied at the external boundaries of our system. The complete external work term is integrated along both the boundary and the applied displacements (u_j);

$$W_{ext} = \iint \sigma_{ij}(u_j, x) u_j \mathrm{d}u_j \mathrm{d}x \quad (4)$$

where σ_{ij} is the stress along the boundary due to u_j and x is position along the external boundary. In a closed system, the total work of the system must equal the external work. In our models, the boundaries are not permitted to move so the external work does not change during rupture propagation; the only changes are the partitioning of work amongst the different work components within the system.

In order for a tectonic fault to slip, the shear stress along the fault must overcome the frictional strength of the fault. The work done against frictional resistance at a single fault segment is calculated as:

$$W_{fric} = \sigma_N \mu s A \quad (5)$$

where σ_N is normal stress, μ is the coefficient of friction, s is slip and A is the ruptured areas of the fault. When stresses along the fault are tensile so that normal stresses are zero or positive, the work done against friction is zero. The complete frictional work in two dimensions is integrated over both the loading path and the length of the fault, l:

$$W_{fric} = \iint \sigma_N(u_i, l) \mu s(u_i, l) \mathrm{d}u_i \mathrm{d}l. \quad (6)$$

Frictional work depends on the coefficient of friction, which in our slip-weakening model changes with increasing displacement. Until the slip-weakening distance is reached, the μ in the frictional work term is a function of displacement. After a displacement equal to L has been achieved, μ is equal to the dynamic friction value. W_{fric} is similar to the E_F notation used by Kanamori and Heaton (2000) to describe the frictional energy loss except that our frictional work integrates over the decrease in shear stress as slip increases from zero to L. E_F only considers the frictional work done under the dynamic shear stress. Consequently, W_{fric} is equivalent to $E_F + E_G$ of Kanamori and Heaton (2000) notation, where E_G represents the energy consumed along the fault as slip increases to the critical slip distance. With our delineation of work terms, the frictional work produced by the rupture is expected to depend on the slip-weakening length of the fault, while the seismological frictional work delineation does not.

The work done in the creation of new surfaces through the nucleation and propagation of off-fault tensile cracks is a function of the surface energy of a crack, G_c, and the total area of new fracture surface created, S.

$$W_{prop} = G_c S \quad (7)$$

The surface energy for rocks has been empirically estimated in a variety of ways through laboratory (e.g. Wong, 1982; Cox and Scholz, 1988) and field analyses (e.g. Olgaard and Brace, 1983; Chester et al., 2005). These estimations provide a wide range of values. Analytically, the propagation energy can be directly calculated from the prescribed fracture toughness because the fractures only grow when the stress intensity factor exceeds the fracture toughness of the rock. The plane strain relationship between energy release rate G_{Ic} and K_{Ic} provides a means to calculate W_{prop}.

$$W_{prop} = SG_{Ic} = S\left(1-\nu^2\right)\frac{K_{Ic}^2}{E} \quad (8)$$

where E and ν are the Young's Modulus and Poisson's ratio respectively of the material. For the material property values chosen for this modeling study ($E = 20$ GPa; $\nu = 0.2$; $K_{Ic} = 2.5$ MPa $m^{1/2}$), the surface energy is 300 J/m^2. This formulation of W_{prop} differs from that of the fracture energy parameter E_G in the Kanamori and Heaton (2000) formulation because we explicitly solve for the surface energy involved in creating the off-fault fractures in the damage zone.

The energy lost to ground shaking during an earthquake is proportional to the shear stress drop during slip. Although our quasi-static model cannot explicitly account for the energy that would go into the seismic waves, we can approximate this term based on the stress drop that occurs during slip-weakening. This stress drop represents the release of some portion of the stored elastic strain that accumulates as a fault is stressed, however stress drop may represent only a small fraction of the total shear stress on the fault. We approximate the seismic energy released during a slip event as:

$$W_{seis} = \iint \Delta\tau(u_j, l)s(u_j, l)\mathrm{d}u_j\mathrm{d}l \quad (9)$$

where $\Delta\tau$ is shear stress drop during slip-weakening. W_{seis} is similar to the E_R in the notation used by Kanamori and Heaton (2000). We will investigate if faults with different roughnesses release different amounts of seismic energy during rupture propagation. Stress drop in a fully dynamic model maybe higher for the given conditions than our model results, but the trends we see in the seismic work for changing slip-weakening distance should be applicable for a fully dynamic model.

The internal work of the fault system is measured strain energy density. Timoshenko and Goodier (1951) derived the total strain energy for a two-dimensional system to be the sum of stress multiplied by strain over an infinitely small increment of strain. The integral of the strain energy over the entire two-dimensional body yields:

$$W_{int} = \iint \frac{1}{2}(\sigma_{xx}\varepsilon_{xx} + \sigma_{zz}\varepsilon_{zz} + 2\sigma_{xz}\varepsilon_{xz})\mathrm{d}x\mathrm{d}z \quad (10)$$

Although the internal strain energy represents elastic (and therefore recoverable) strain, the internal work term also represents the energy available for consumption by inelastic processes such as the production of off-fault damage. Prior to any slip along the fault, $W_{fric} = W_{prop} = W_{seis} = 0$ so that W_{int} equals external work. We expect that W_{int} will decrease with slip and damage production along the modeled faults. In our study, the internal work is sampled at observation points distributed throughout the model. These observation points often fall within areas of concentrated stresses near the tips of the off-fault damage. Near the displacement discontinuity elements, the local stress singularity is overestimated (i.e. r^{-1} instead of $r^{-1/2}$) so that sampling in these regions produces artificially high internal work. A more reliable method of calculating W_{int} is to subtract the other work terms from W_{ext}.

3. Results

3.1. Slip-weakening distance and off-fault fracture patterns

We compare the off-fault fracture patterns and slip profiles generated along faults with varying slip-weakening distances due to the application of displacements at the boundaries of our model (Fig. 2). The fracture patterns are shown for each fault at the time when the rupture reaches the tip of the modeled fault. New fractures develop perpendicular to the direction of greatest tensile stress and at positions along the fault where local tensile stress exceeds tensile strength. This occurs at the rupture front where an element that slipped juxtaposes an element that has not; the high slip gradient produces locally high tension on one side of the fault. Fractures form mostly in the tensile quadrants of the rupture tip and sub-perpendicular (approximately 70–85°) to the fault. In some cases, a few cracks develop in the overall compressive quadrants of the fault when local tensions arise during rupture. As new fracture tips continue to propagate, they grow in various directions, highlighting the locally changing stress fields due to the presence of other nearby fractures. The resulting sawtooth fracture trace is element size dependent, however the average fracture angle for a given crack is not. The lack of perfect symmetry in the fracture pattern arises from slight asymmetry in boundary conditions to prevent rigid body motion. Once a small degree of fracture asymmetry is introduced, the asymmetry of the model is further enhanced.

Faults with the longest L (Fig. 3A) show fracture patterns resembling static friction fault models (Martel, 1997) where fractures are located in the tensile quadrants at the fault tips. Decreasing the slip-weakening length creates more fracturing inboard of the fault tip, resembling fully dynamic models of tensile fracture zones, with the fractured area forming a wedge shape that tapers towards the center of the fault when new fractures are allowed to continue to grow after the rupture has reached the fault tip (Fig. 3B; Dalguer et al., 2003). This same wedge-shaped pattern is predicted by analytical models that predict zones of activated off-fault damage but do not explicitly generate off-fault fractures (Andrews, 2005; Rice et al., 2005; Templeton and Rice, 2008). However for our comparison, we restrict our analysis of the fracture patterns to the iteration at which the rupture reached the fault tip. Because the models presented here, as well as other models of off-fault damage, do not allow for the fault tip to propagate when the rupture reaches the fault tip, the resulting off-fault damage pattern may not be meaningful past this iteration.

The initial fault roughness (i.e. the slip-weakening distance) has a large effect on resultant fracture density and clustering of the damage zone (Fig. 2). Fracture density along the length of the fault decreases as a function of increasing slip-weakening distance (Fig. 4). The fractures form in clusters, with the number of clusters decreasing with larger slip-weakening distances. The clusters represent deviations in the slip profile from ellipticity. For longer slip-weakening distances, the slip profile along the fault maintains a mostly elliptical shape (Fig. 2). However, as L decreases, small "toes" of slip extend from the rupture front that represent the number of elements whose frictional strength is falling from the static to the dynamic value in that iteration (Fig. 4B; online supplementary material). The clusters form between the element closest to the tip that has weakened to its dynamic friction value and the elements along which friction is

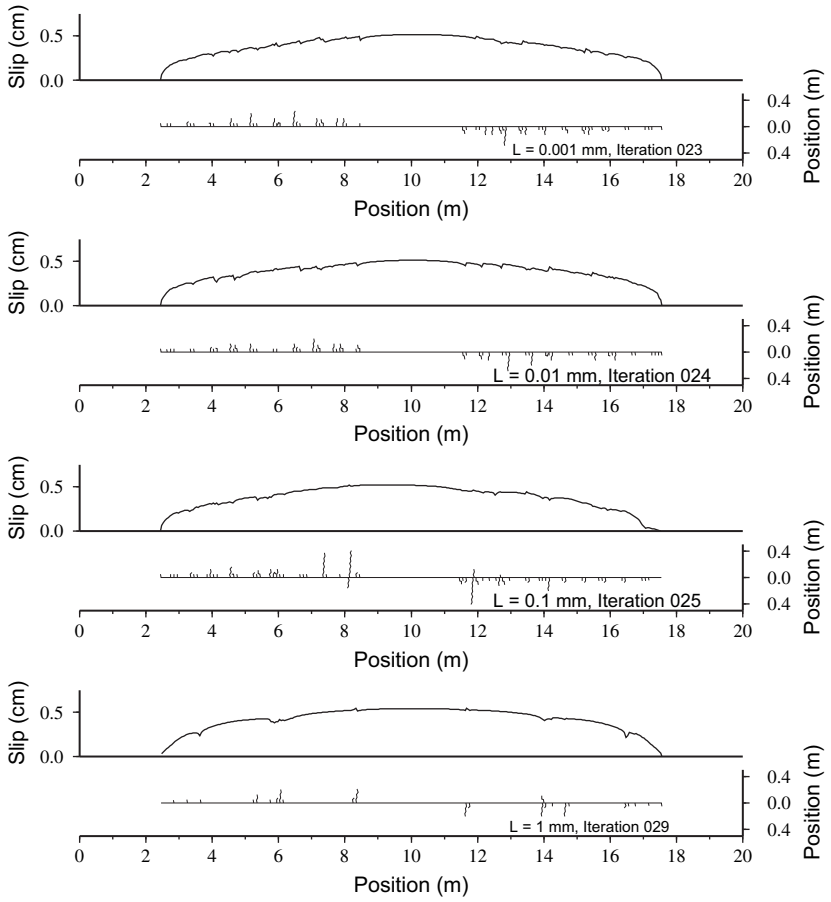

Fig. 2. Fracture patterns and slip profiles generated along faults of varying slip-weakening distances: A) 0.001 mm, B) 0.01 mm, C) 0.1 mm, and D) 1 mm. Faults are compared at the iteration at which the rupture front reaches the end of the fault. More off-fault damage occurs on smoother faults.

falling. When the slip-weakening distance is small, fewer elements are in transition between static and dynamic friction, resulting in damage clusters that are closer together. The growth length of fractures in a single iteration and spacing of the clusters depend on element size, but not the pattern of clustering.

Smaller slip-weakening distance means that elements reach dynamic friction levels more quickly and the rupture reaches the fault tip in fewer iterations for the smoother faults (Fig. 5). The increased time spent slipping at higher coefficients of friction slows the rupture speed on the rougher faults. The fault rupture propagates on the order of centimeters per iteration, which can be thought of as a unit of time. The growth of mode I fractures can grow one element per iteration, which in these models is 5 cm. Therefore the Mode II rupture speed is similar to the Mode I propagation speed in these models.

An interesting point to note is that although aspects of the slip patterns vary while the rupture is propagating, the final slip profiles, as well as average and maximum slip values, are very similar (Fig. 2). According to our models, faults with similar slip

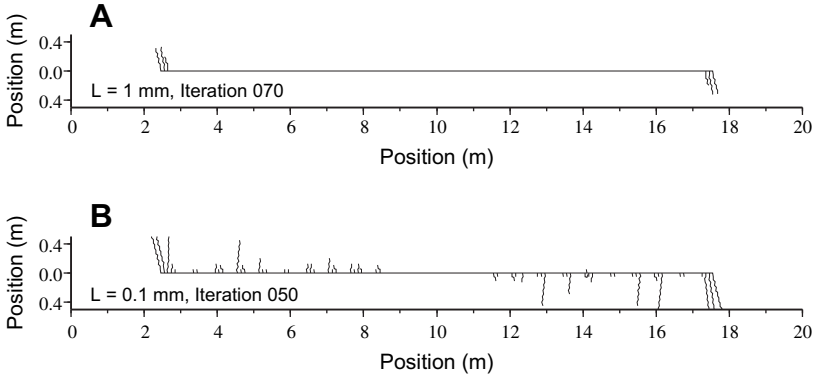

Fig. 3. Faults allowed to continue fracturing after the rupture reached the fault tip show that faults with small slip-weakening distances resemble models of static friction (A) and faults with longer slip-weakening distances resemble models of dynamic slip (B).

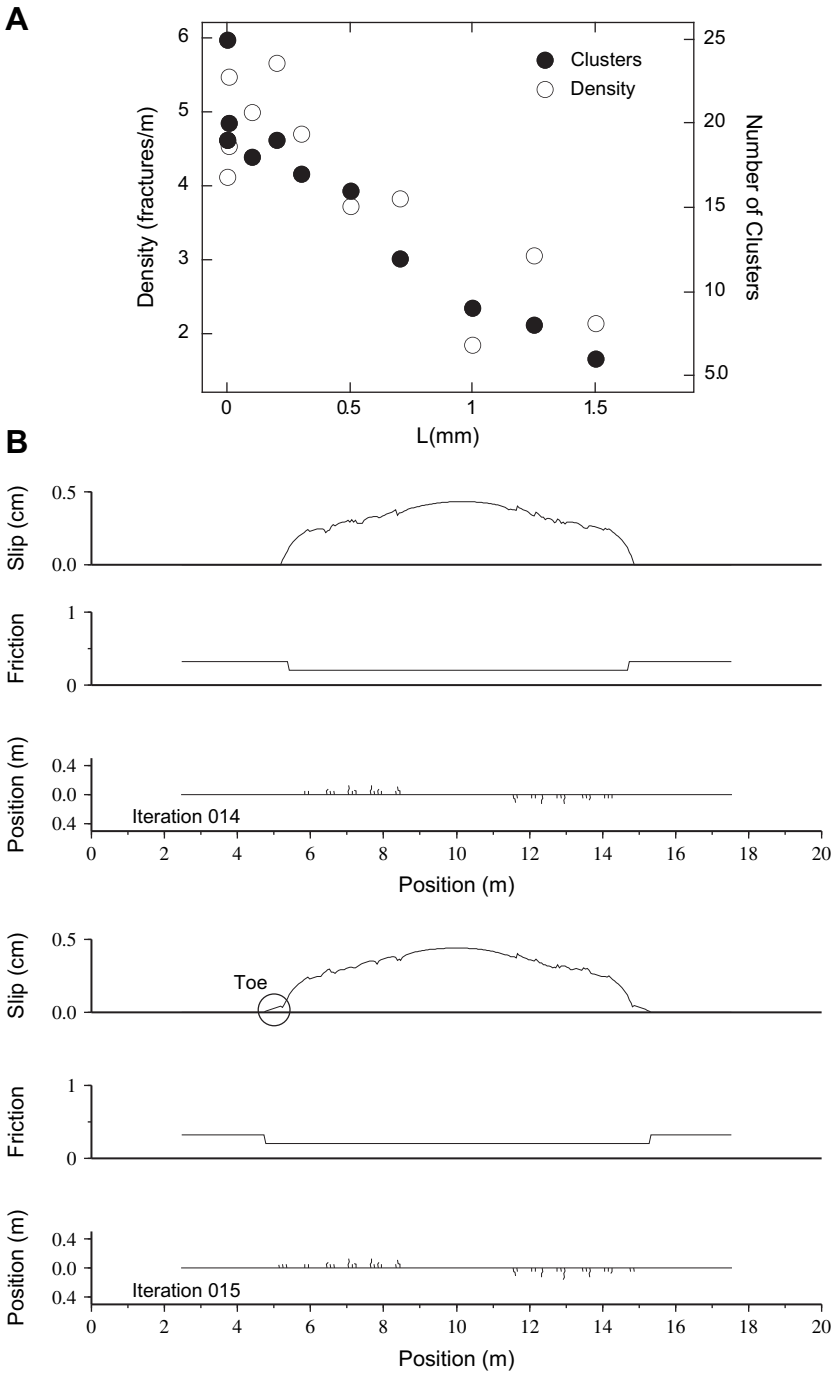

Fig. 4. A) Along-strike fracture density decreases as a function of slip-weakening distance. This trend results in less continuous damage along the fault, so that there are fewer clusters of fractures. B) Clustering is a function of slip-weakening distance because it represents the length of the transition zone from locked to slipping, and therefore the region that is subjected to local tensile stress. This region can be seen as a "toe" on the slip profile in Iteration 15.

profiles but different initial surface roughness would have very different fracturing intensity within the damage zone, at least for the initial stages of damage zone development. The maximum width of the damage zone is similar between all models, and damage zones are wider per unit of slip than predicted by fault scaling models (Scholz, 2002).

3.2. Mechanical work

In an effort to assess the mechanical efficiency of the fractured fault zones, we analyze the mechanical work associated with a variety of slip-weakening distances along the modeled faults. We examine both the components of work when the rupture reaches the tip of each fault, as well as how different components of the total work change as the rupture propagates.

3.2.1. Change in work with rupture propagation

We investigate how the work against frictional resistance and seismic energy release components of the work budget evolve throughout the rupture process. Fig. 6 shows how frictional and seismic work increase over the course of a slip event in two models with differing slip-weakening lengths. At the onset, no slip has

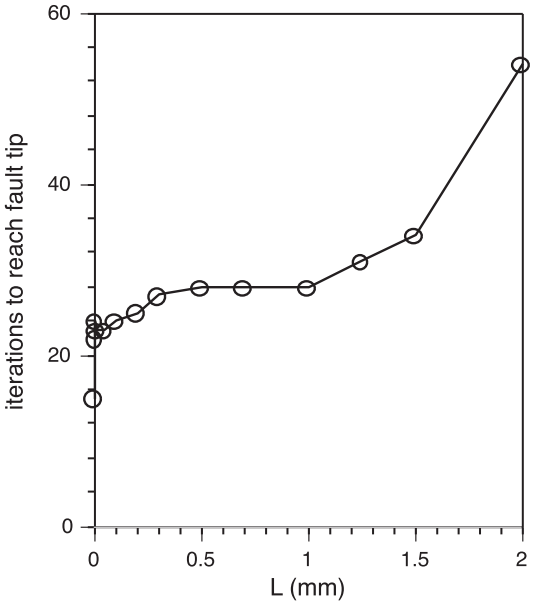

Fig. 5. Iterations to the modeled fault tip for faults with differing slip-weakening distance, *L*. Rupture propagates more slowly on rougher faults and takes more iterations to reach the fault tip.

occurred and therefore no work has gone into friction or seismic energy; all of the external work is expressed as internal work within the material surrounding the fault. As slip progresses, W_{fric} and W_{seis} increase at the expense of internal work. The smoother fault produces greater seismic work and greater frictional work at each iteration of fault slip (Fig. 6). The seismic work and frictional work are generated not just on the main fault but also along the off-fault fractures as they slide. This accounts for irregularities along the curves in Fig. 6. Because the rougher fault ($L = 1$ mm) takes 4 more iterations than the smoother fault ($L = 0.01$ mm) to reach the fault tip, the frictional work on the rough fault slightly exceeds that of the smooth fault once the rupture is at the tip of both modeled faults.

3.2.2. Sensitivity of work components to slip-weakening distance

The total work of fracture propagation scales with the length/area of new fracture surface produced (Eq. (9)). Faults with longer slip-weakening distance produce less off-fault damage and consume less work of fracture propagation (Fig. 7). The anomalously large damage produced by the model with $L = 1$ mm is due to tensile fractures that develop within the compression quadrant of this fault.

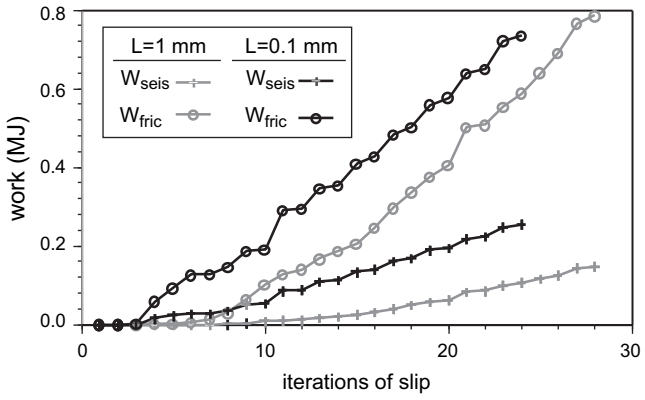

Fig. 6. Increase of work against frictional resistance to sliding (W_{fric}) and work of seismic energy release (W_{seis}) during iterations of slip along two faults with different slip-weakening distance, *L*. At each iteration of rupture propagation, W_{fric} and W_{seis} for the smoother fault exceed the work of the rough fault. Once rupture reaches both modeled fault tips, the fictional work is slightly greater for the rougher fault.

The work against frictional resistance to sliding and the seismic radiated energy are plotted for faults when the rupture has just reached the ends of the modeled faults. At this point, each of the models has similar slip profile. The frictional work increases modestly with increasing slip-weakening distance. Although faults with $L = 1$ mm have greater off-fault damage than faults with $L = 2$ mm, the $L = 1$ mm faults require less frictional work. Frictional work depends on both slip and friction coefficient. Because the fault with longer slip-weakening distance slips while the friction coefficient is higher than the fault with shorter *L*, the fault with longer *L* requires greater frictional work. Rough faults may require slightly greater frictional work to slip than smoother faults; however these differences may be small and impossible to discern in the field. In addition to slip and friction coefficient, frictional work also depends on normal stress (Eq. (6)). While the normal stress is the same for the faults modeled, it may differ significantly for faults in the field.

The seismic radiated energy calculated from shear stress drops, along both the primary fault and along the off-fault damage, decreases sharply with increasing slip-weakening distance (Fig. 7b). With smooth faults, the coefficient of friction and subsequently the shear stress can have greater drop between iterations than along faults with long slip-weakening distance. The larger shear stress drops between rupture propagation iterations produces larger seismic radiated energy. Augmenting this trend is the tendency for faults with smaller *L* to produce greater damage (Fig. 7c). The development of off-fault fractures provides a means to transfer stored internal work to seismic radiated energy. Together these processes imply that rupture along smoother faults should produce more shaking than ruptures along rougher faults.

3.3. Second generation of damage

Our model results suggest that fault surface evolution should be accompanied with greater production of damage, slightly lesser frictional work and significantly greater seismic energy release. These trends neglect the influence of pre-existing off-fault damage. To begin to address this issue we investigate the propagation of rupture and development of damage along a fault that already has some off-fault damage. We use the fracture pattern from the $L = 1.5$ mm fault for the initial damage pattern and reapply the boundary conditions. Before we allow the rupture to start along the central weak patch, we first apply the boundary displacements and let the faults slip and the cracks grow to their full extent under the applied loading. Once this is complete, the friction on all faults is brought to the static friction levels and the friction along the central patch lowered to induce rupture.

Table 1 presents the number of iterations to reach the modeled fault tip and work values for the first and second rupture episodes along the $L = 1.5$ mm fault. The number of slip iterations for the rupture to reach the fault tip increases when the fault is flanked by existing fractures. The pre-existing damage deforms as the rupture propagates along the fault, slowing down the rupture. Fracture clusters from the first episode are made longer but few new clusters form (Fig. 8; online supplement). The growth of fractures per unit slip also increases; whereas the total slip on the fault doubles when adding the two episodes, the length of the longest fractures quadruples. The total length of damage increases, which is reflected in the near doubling of the work of fracture propagation. The presence of off-fault damage also increases the seismic radiated

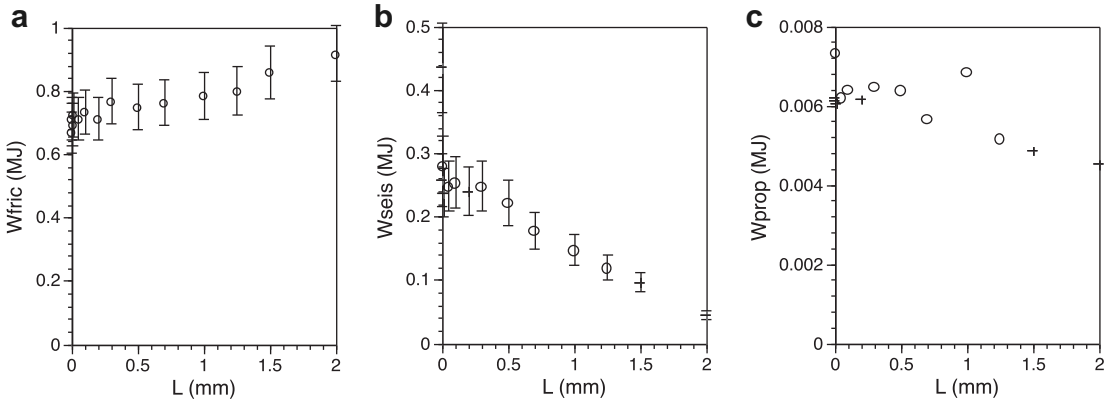

Fig. 7. Sensitivity of (a) frictional work, (b) and seismic energy and (c) propagation energy with slip-weakening distance along the modeled faults. We calculate the error of the work values by examining the difference in work between these models and models with twice the element size. Open symbols denote models that produced tensional cracks within the contractional quadrants of the fault. Frictional work increases slightly with L whereas seismic work decreases dramatically with increasing slip-weakening distance. The amount of damage decreases with slip-weakening distance.

energy by a small amount compared to the first episode of slip. The internal work calculated by subtracting all the other work terms from the external work decreases slightly with the second episode of slip.

4. Discussion

4.1. Fracture patterns

The qualitative analysis of the off-fault damage pattern resulting from fault slip has some interesting applications for field observations. The models show that the initial surface roughness on the fault will have a considerable effect on the continuity of the damage zone along strike. Faults with smaller slip-weakening distances would have a more continuous damage zone, whereas faults with large slip-weakening distances would have a less dense network of fractures. However, we should note that a fault that has greater geometric roughness (non-planarity) would concentrate damage at asperities. The formation of off-fault damage diminishes slip on the adjacent fault patch from an expected elliptical slip distribution. The absolute magnitude of the critical slip distance is difficult to assess for tectonic faults. In the laboratory, where surfaces in general are smooth and gouge zone thicknesses in the millimeter range, critical slip distance values are generally measured to be 10 s of microns with the expectation of scaling up to earthquake faults. Seismic slip inversions have estimated the critical slip distance on the order of 10–100 cm. Although critical slip distance should generally decrease as fault motion wears down asperities (Sagy et al., 2007), the difficulty of measuring the evolution of this parameter in nature hampers our understanding of these processes.

Table 1
Pre-existing fractures slow the speed of rupture and alter the work budget. More work goes into seismic radiation and fracture propagation, whereas damage decreases frictional work.

	#Iterations to fault tip	W_{seis} (MJ)	W_{fric} (MJ)	W_{prop} (MJ)	W_{int} (MJ)
$L = 1.5$ mm first	34	0.10	0.86	0.0049	41.34
$L = 1.5$ mm second	48	0.14	0.84	0.0075	41.31

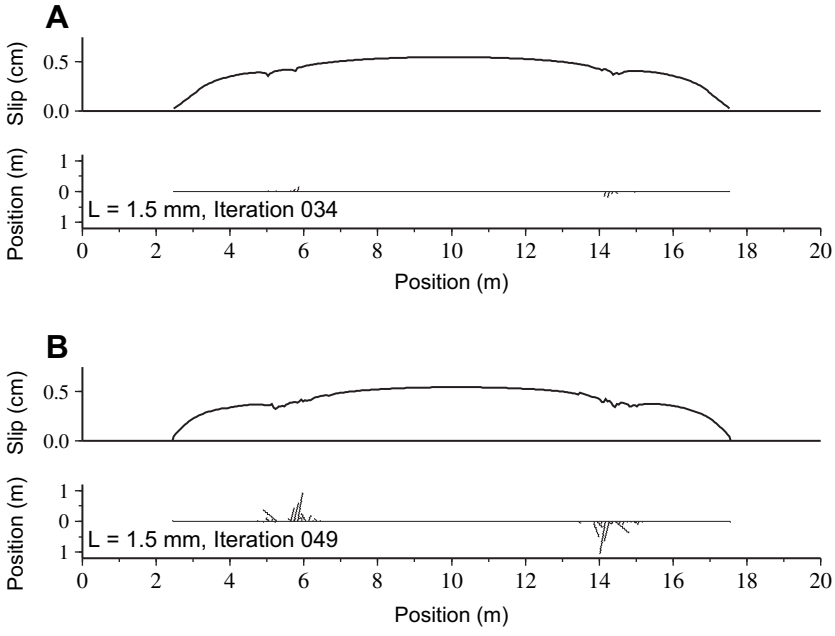

Fig. 8. Fault with pre-existing damage subjected to second episode of slip shows enhanced damage in areas where damage had already localized, but little new fracturing.

The models demonstrating the second generation of slip imply that faults in the field with more than one slip episode will have high density, clustered fracture patterns, due to the ease of propagating a fracture relative to forming a new one. This results in a larger ratio between damage zone width and slip than a fault that has one slip episode where total slip equaled the sum of the two smaller episodes. However, using damage zone width per unit of slip to estimate number of slip events would need to be limited to comparing faults within the same field site. Additionally, significant interseismic healing of fractures through processes such as mineral precipitation would mitigate the effect of pre-existing damage on subsequent ruptures.

4.2. Mechanical work analysis

Within the models of this study, we hold the external work constant; no additional work is added to the system during the propagation of the rupture. Because the left hand side of Eq. (3) is constant during slip, the changes in work that we observe in the models reflects the transfer of work from internal stored work to the non-conservative frictional heating, seismic radiated energy and propagation energy. Of these non-conservative terms, the greatest work is consumed in frictional heating along the primary fault and its damage structures. In contrast, the work of fracture propagation is several orders of magnitude smaller than the other work terms, however processes such as rock pulverization could require much more propagation energy than the cracks formed in these models (Wilson et al., 2005). The total work of the system is about 42.3 MJ so by far the greatest component of work is the internal work stored within the system. Within these models only 2% of the internal work is converted to non-conservative work terms. Our models show that internal work decreases slightly upon the second episode of slip along the fault. This suggests that further ruptures along the fault could continue to transfer stored energy within the host rock into frictional heating, seismic radiated energy and the creation of new fault surfaces. With successive rupture events we expect the slip-weakening distance along the fault to generally decrease. Smoother faults are more effective than rough faults at transferring work from internal work to the non-conservative work terms.

5. Conclusions

Two-dimensional linear elastic models of frictional faults suggest that the frictional slip-weakening distance (L) has significant effects on the tensile, off-fault damage pattern in a fault zone. Faults with smaller slip-weakening distance have more continuous along-strike damage whereas faults with large slip-weakening distances concentrate fracturing at fault tips. Fractures form along the fault in small clusters, with the number of clusters increasing as function of L, thereby making along-strike fracturing more continuous. Slip-weakening distance also affects how work is consumed within the fault zone, with longer slip-weakening distance resulting in more work done against friction and less radiated seismic energy. Pre-existing damage further localizes fracturing and consumes more internal work. Because initial damage may be related to fault roughness, this implies that incipient fault roughness controls along-strike fracture density even after many episodes of slip.

Acknowledgements

We would like to thank two anonymous reviewers whose insights greatly improved the paper. This work was supported by NSF Grant EAR-0349070 to Michele Cooke.

Appendix. Supplemental data

Supplemental data associated with this article can be found in online version at doi:10.1016/j.jsg.2009.08.014.

References

Abercrombie, R.E., Rice, J.R., 2005. Can observations of earthquake scaling constrain slip-weakening? Geophysical Journal International 162. doi:10.1111/j.1365-246X.2005.02579.x.
Andrews, D.J., 2005. Rupture dynamics with energy loss outside the slip zone. Journal of Geophysical Research 110. doi:10.1029/2004JB003191.
Broberg, K.B., 1999. Cracks and Fractures. Academic Press, San Diego.
Brock, W.G., Engelder, J.T., 1977. Deformation associated with the movement of the Muddy mountain overthrust in the Buffington window, southeastern Nevada. Bulletin of the Geological Society of America 88, 1667–1677.
Burgmann, R., Pollard, D., Martel, S., 1994. Slip distributions on faults: effects of stress gradients, inelastic deformation, heterogeneous host-rock stiffness, and fault interaction. Journal of Structural Geology 12, 1675–1690.
Caine, J.S., Evans, J.P., Forster, C.B., 1996. Fault zone architecture and permeability structure. Geology 24, 1025–1028.
Chester, F.M., Logan, J.M., 1986. Implications for mechanical properties of brittle faults from observations of the Punchbowl Fault, California. Pure and Applied Geophysics 124, 77–106.
Chester, J.S., Chester, F.M., Kronenberg, A.K., 2005. Fracture surface energy of the Punchbowl fault, San Andreas system. Nature 437. doi:10.1038/nature03942.
Cooke, M.L., 1997. Fracture localization along faults with spatially varying friction. Journal of Geophysical Research 102, 22,425–422,434.
Cooke, M.L., Murphy, S., 2004. Assessing the work budget and efficiency of fault systems using mechanical models. Journal of Geophysical Research 109. doi:10.1029/2004JB002968.
Cowie, P.A., Shipton, Z.K., 1998. Fault tip displacement gradients and process zone dimensions. Journal of Structural Geology 20, 983–997.
Cox, S.J.D., Scholz, C.H., 1988. Rupture initiation in shear fracture of rocks: an experimental study. Journal of Geophysical Research 93 (B4), 3307–3320.
Crouch, S.L., Starfield, A.M., 1990. Boundary Element Methods in Solid Mechanics. Unwin Hyman, Boston, Mass.
Dalguer, L.A., Irikura, K., Riera, J.D., 2003. Simulation of tensile crack generation by three-dimensional dynamic shear rupture propagation during an earthquake. Journal of Geophysical Research 108. doi:10.1029/2001JB001738.
Del Castello, M., Cooke, M.L., 2007. The underthrusting-accretion cycle: work budget as revealed by the boundary element method. Journal of Geophysical Research 112, B12404. doi:10.1029/2007JB004997.
Dieterich, J.H., 1979. Modeling of rock friction: 1. Experimental results and constitutive equations. Journal of Geophysical Research 84, 2161–2168.
Faulkner, D.R., Mitchell, T.M., Healy, D., Heap, M.J., 2006. Slip on 'weak' faults by the rotation of regional stress in the fracture damage zone. Nature 444. doi:10.1038/nature05353.
Ismat, Z., 2008 Energy budget during fold tightening of a multilayer fold. Journal of Structural Geology 31. doi:10.1016/j.jsg.2008.10.006.
Kanamori, H., Heaton, T.H., 2000. Microscopic and macroscopic physics of earthquakes. In: Rundle, J., Turcotte, D., Klein, W. (Eds.), Geocomplexity and the Physics of Earthquakes. Geophysical Monograph, vol. 20. American Geophysical Union, Washington D.C., pp. 127–141.
Kim, Y.-S., Peacock, D.C.P., Sanderson, D.J., 2004. Fault damage zones. Journal of Structural Geology 26, 503–517.
Maerten, L., Willemse, E.J.M., Pollard, D.D., Rawnsley, K., 1999. Slip distributions on intersection normal faults. Journal of Structural Geology 21, 259–271.
Manighetti, I., King, G., Sammis, C.G., 2004. The role of off-fault damage in the evolution of normal faults. Earth and Planetary Science Letters 217. doi:10.1016/S0012-821X(03)00601-0.
Marone, C., Kilgore, B., 1993. Scaling of the critical slip distance for seismic faulting within shear strain in fault zones. Nature 362. doi:10.1038/362618a0.
Marshall, S.T., Cooke, M.L., Owen, S.E., 2008. Effects of non-planar fault topology and mechanical interaction on fault slip distributions in the Ventura basin, CA. Bulletin of the Seismological Society of America 98, 1113–1127. doi:10.1785/0120070159.
Martel, S.J., 1997. Effects of cohesive zones on small faults and implications for secondary fracturing and fault trace geometry. Journal of Structural Geology 19, 835–847.
Mitra, G., Boyer, S.E., 1986. Energy balance and deformation mechanisms of duplexes. Journal of Structural Geology 8, 291–304.
Okubo, C.H., Schultz, R.A., 2005. Evolution of damage zone geometry and intensity in porous sandstone: insight gained from strain energy density. Journal of the Geological Society of London 162, 939–949.
Olgaard, D.L., Brace, W.F., 1983. The microstructure of gouge from a mining-induced seismic shear zone. International Journal of Rock Mechanics and Mining Sciences and Geomechanics Abstracts 20, 11–19.
Ohnaka, M., 2000. A physical scaling relation between the size of an earthquake and its nucleation zone size. Pure and Applied Geophysics 157, 2259–2282.
Rice, J.R., Sammis, C.G., Parsons, R., 2005. Off-fault secondary failure induced by a dynamic slip pulse. Bulletin of the Seismological Society of America 95, 109–134.
Rispoli, R., 1981. Stress fields around strike-slip faults inferred from stylolites and tension gashes. Tectonophysics 75, T29–T36.

Ruina, A., 1983. Slip instability and state variable friction laws. Journal of Geophysical Research 88, 10359–10370.
Sagy, A., Brodsky, E.E., Axen, G.J., 2007. Evolution of fault surface roughness with slip. Geology 35, 283–286.
Savage, H.M., Cooke, M.L., 2004. An investigation into the role of fault interaction on fold pattern. Journal of Structural Geology 26, 905–917.
Scholz, C.H., 2002. The Mechanics of Earthquakes and Faulting. Cambridge University Press, New York.
Shipton, Z.K., Cowie, P.A., 2003. A conceptual model for the origin of fault damage zone structures in high-porosity sandstone. Journal of Structural Geology 25, 333–344.
Sibson, R.H., 1977. Fault rocks and fault mechanisms. Journal of the Geological Society 133, 191–213.
Stein, R.S., 1999. The role of stress transfer in earthquake occurrence. Nature 402, 605–609.
Templeton, E.L., Rice, J.R., 2008. Off-fault plasticity and earthquake rupture dynamics: 1. Dry materials or neglect of fluid pressure changes. Journal of Geophysical Research 113. doi:10.1029/2007JB005529.
Timoshenko, S.P., Goodier, J.N., 1951. Theory of Elasticity. McGraw-Hill, New York.
Willemse, E.J.M., Pollard, D.D., Aydin, A., 1996. Three-dimensional analyses of slip distributions on normal fault arrays with consequences for fault scaling. Journal of Structural Geology 18 295–209.
Wilson, B., Dewars, T., Reches, Z., Brune, J., 2005. Particle size and energetics of gouge in from earthquake rupture zone. Nature 434, 749–752.
Wong, T.-f., 1982. Shear fracture energy of westerly granite from postfailure behavior. Journal of Geophysical Research 87, 990–1000.
Yamashita, T., 2000. Generation of microcracks by dynamic shear rupture and its effects on rupture growth and elastic wave radiation. Geophysical Journal International 143, 395–406.